Engineering Structures 351 (2026) 122050

Contents lists available at ScienceDirect

Engineering Structures

journal homepage: www.elsevier.com/locate/engstruct

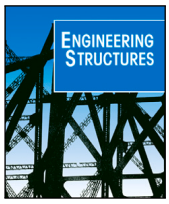

Experimental and probabilistic analysis of masonry cavity wall ties under out-of-plane loading with application of stochastic numerical analyses

Chee Yin Lam [a,*], Lewis J. Gooch [b], Mark J. Masia [a], Igor A. Chaves [a]

[a] Critical Infrastructure Performance and Reliability Group, The University of Newcastle, University Dr, Callaghan, Newcastle, 2308, NSW, Australia
[b] College of Science and Engineering, James Cook University, 1 James Cook Drive, Douglas, Townsville, 4811, QLD, Australia

ARTICLE INFO

Keywords:
Cavity wall tie
Probabilistic model
Spatial variability
Stochastic finite element analysis

ABSTRACT

Most existing studies on wall tie material characterisation are deterministic, and the random variability of tie behaviour which arises from the tie material, mortar quality and tie installation process were not studied extensively. This study presents the results of a probabilistic characterisation of corrugated-end cavity wall ties and a spatially variable stochastic finite element analysis of one-storey cavity wall subjected to out-of-plane loading, considering variable properties for the wall ties and masonry. The tie strengths were first tested according to AS2699.1:2020, resulting in an idealised load–displacement curve capable of describing the compressive and tensile behaviour of the tie. Suitable predictive models for the characteristic points of the idealised curve were determined by considering the goodness-of-fit of a range of probabilistic distributions, allowing the random variations in the derived cavity wall tie constitutive model to be considered. The numerical results indicated that inward loading was governed by tie failure, whereas outward loading was governed by masonry tensile cracking. Further spatial stochastic simulations indicated that the mean peak load under inward loading was 2.6% lower than the deterministic baseline of 5.46 kPa, with a COV of 0.06. While the mean peak load under outward loading was 1.4% higher than the deterministic baseline of 4.96 kPa, with a COV of 0.04. The findings provide novel insights into the development of probabilistic tie constitutive model, the interaction of spatially variable components in cavity wall systems and the subtle difference in load-sharing mechanisms under different out-of-plane loading conditions, with implications for further reliability assessment and design safety.

1. Introduction

Masonry structures are commonly built in Australia for residential and low-rise commercial buildings. In particular, masonry cavity and veneer walling systems are often utilised for their robustness, durability and thermal performance. Both types of construction use wall ties to connect the outer wythe of the brick wall to the inner load-bearing elements to ensure that horizontal loads are transferred safely under wind or earthquake loading conditions. Given the importance of wall ties as connectors in maintaining structural integrity of masonry structures, many researchers have conducted experimental characterisation tests of wall ties under different loading conditions [1–7]. Focusing on cavity wall ties, Arslan et al. [6] characterised the axial behaviour of two different cavity wall ties under the influence of various installation and loading configurations, and a subsequent study by the same authors [7] proposed a mechanical model aimed at estimating the strength capacity of cavity wall ties and predicting failure modes.

However, most existing studies on wall tie characterisation are deterministic in nature, the random variability in wall tie material, mortar quality and the tie installation process was not extensively quantified [8,9]. By utilising randomly variable material properties, in place of mean or characteristic values, a finite element analysis may capture the variability in a structure's response to loading. Furthermore, by considering a spatially variable model, localised failures within a structural system may be captured, allowing for more accurate predictions of structural resistance. For this purpose, the application of stochastic finite element modelling approach has received increasing interest to account for the significant material and construction variability of masonry structures. Previous studies on spatially variable material properties [10–13] have contributed to an improved understanding of how non-homogeneity material influences the structural reliability of masonry structures. Li et al. [14,15,16] investigated the impact of spatial variability in flexural tensile strength on the cracking and peak loads of unreinforced masonry panels subjected to one-way and two-way bending. By considering spatial variability of flexural tensile strength on a joint-by-joint basis, it was concluded that a higher

* Corresponding author.
E-mail address: CheeYin.Lam@uon.edu.au (C.Y. Lam).

https://doi.org/10.1016/j.engstruct.2025.122050
Received 4 August 2025; Received in revised form 19 December 2025; Accepted 23 December 2025
Available online 2 January 2026

accuracy of load capacity estimation can be achieved, leading to closer agreement with experimental observations.

In addition, the research conducted by Muhit et al. [8] is of particular relevance, who quantified the random variability of masonry veneer wall ties by testing 50 brick-tie-timber subassemblies under tension and compression. Based on the observed behaviour of the veneer wall ties, a probabilistic constitutive law of the veneer wall tie was proposed since the ideal elastic–plastic model was not accurate enough to capture the tie behaviour. By considering the random variability of the tie behaviour and other masonry properties, spatial stochastic finite element analyses were conducted. The stochastic approach using probabilistic material models was more accurate in terms of modelling the failure progression and matching the peak out-of-plane loading capacity observed in laboratory tests [17]. In contrast, the deterministic modelling approach overestimated the loading capacity, highlighting the importance of developing probabilistic material models and applying stochastic numerical analyses to evaluate the structural reliability of masonry structures. Apart from improving the understanding of structural reliability of masonry structures by considering material variability, the outputs generated from SFEA can be further utilised to train machine learning models with the goal of predicting the failure modes and pull out force of metal anchors in masonry structures, as demonstrated in [18], highlighting the broader value of SFEA in enabling a data-driven prediction framework.

Given that wall ties come with various shapes and material types as the design standards and construction practices have evolved over time, this paper aims to characterise the mechanical performance of corrugated-end wall ties in masonry cavity wall systems. Through a series of brick-tie-brick subassembly tests under axial tension and compression, random variability in the behaviour of cavity wall ties was investigated. A probabilistic model of wall tie resistance, capable of capturing the out-of-plane behaviour of masonry cavity wall systems was then developed and implemented into a stochastic finite element analysis to further understand the influence of material variability on loading capacity of masonry cavity wall systems. The remainder of the paper is structured as follows. Section 2 presents the experimental setup and procedures of the cavity wall tie test, while Section 3 details the development of the probabilistic cavity wall tie model. Section 4 describes the finite element modelling strategies and discusses the results of the deterministic and stochastic numerical analyses, and Section 5 concludes the study with key findings and recommendations for future research.

2. Experimental testing program

2.1. Material specifications

In this study, stainless steel, corrugated-end cavity wall ties were selected. The ties were classified as medium-duty strength with a durability class of R4 based on the corrosion resistance required in coastal and industrial areas according to AS3700:2018[19] and AS2699.1:2020 [20]. The dimensions of the tie are shown in Fig. 1, where the corrugation pitch was 12.5 mm, and the tie thickness was specified as 0.95 mm according to the manufacturer.

A total of 20 brick-tie-brick subassemblies were built and each sample was made up of two brick couplets with cavity wall tie as the connector. The brick couplets were constructed using cored clay bricks with standard dimensions of 230 mm long by 110 mm wide by 76 mm high, and bonded using a standard mix of general-purpose M3 mortar [19], with a composition of 1:1:6 (cement: lime: sand, by volume) (approximately 1:0.5:7.6, by mass). The corrugated ends of the tie were embedded in the 10 mm thick mortar joints, forming a cavity width of 50 mm. A schematic diagram of the brick-tie-brick subassembly is shown in Fig. 2.

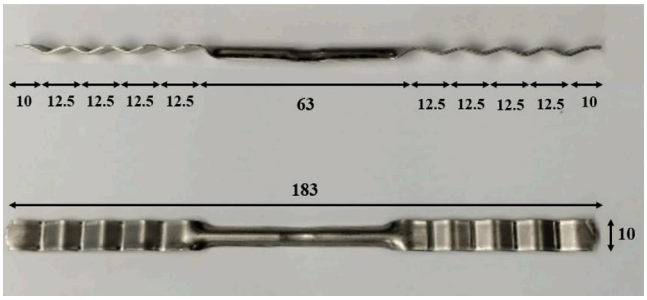

Fig. 1. The dimensions of the selected cavity wall tie (dimensions are in mm).

2.2. Test setup

The brick-tie-brick subassemblies were cured in accordance with AS3700:2018, where the specimens were covered with vapour-proof tarp and left undisturbed for at least 14 days. The curing conditions were not continuously monitored but the average temperature and humidity over the curing period were 18.3 °C and 68% respectively. An electromechanical universal testing system was used to load the samples under both compression and tension. The samples were loaded in a vertical position, where the brick couplets were clamped with a grip system as shown in Figs. 3 and 4 for compression and tension loading conditions respectively. Additional restraining bars were used to secure the samples that were tested in tension to avoid slippage of the samples and compromising the displacement readings. The testing method was designed in accordance with AS2699.1:2020, but a 5 mm vertical offset required by the test method was not implemented to better reflect the as-built conditions of a full-scale cavity wall that has been built without any offset, which is part of an ongoing study at The University of Newcastle. Monotonic axial load was applied to the samples with a displacement rate of 1 mm/min for both compression and tension loading conditions.

Two potentiometers were secured using magnetic bases and mounted on the front and back of the sample. During the compression test, the base of the universal testing machine remained stable and negligible movement was measured, as evident by observing a linear trend of displacements from the potentiometers that closely matched the machine displacement. Therefore, the average displacement recorded from the potentiometers was used as the primary displacement reading for the compression loading case. In contrast, a non-linear trend of displacements was recorded from the potentiometers at the start of the tension test, indicating the occurrence of movement unrelated to the cavity displacement such as the non-negligible base movement of the testing machine. Further sensor over-range issue occurred when the tension test was extended to study the residual effect of the complete wall tie pullout mechanism, causing the data recorded from the potentiometers to be invalid over the 50 mm range. Hence, the machine displacement was deemed more reliable for the tension loading case, and was utilised in the subsequent calculations.

2.3. Compression test results

A total of 10 samples were tested under compression, and the most common failure mode was that of axial buckling of the tie, as demonstrated in Fig. 5a. One sample exhibited a slightly different buckling failure mechanism, where buckling of the tie occurred at the interface of the mortar joint first before buckling in the middle section of the tie. This alternate buckling mode was due to the eccentricity between brick couplets as shown in Figs. 5b and 5c. The resultant load–displacement curve exhibited two distinct peaks. Furthermore, while most of the ties failed by buckling, one of the samples failed by piercing of the tie in the mortar as shown in Fig. 6. The piercing failure mode

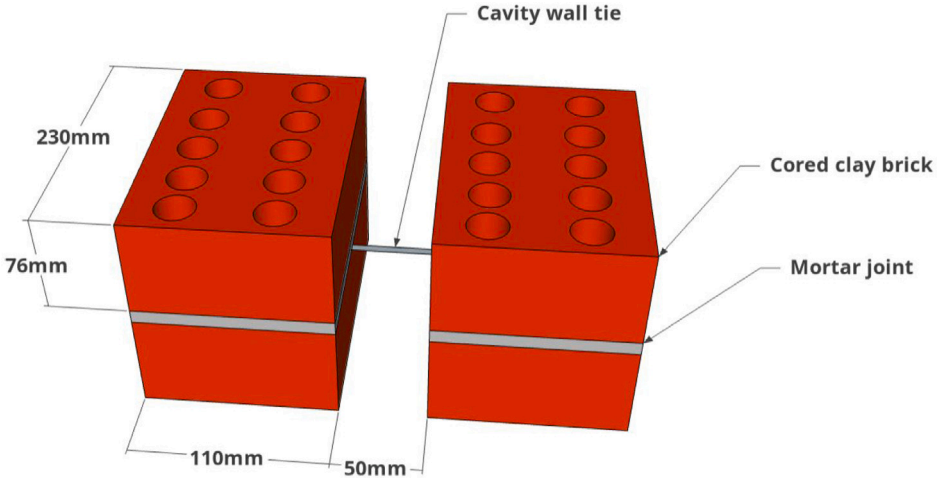

Fig. 2. Schematic diagram of the brick-tie-brick subassembly.

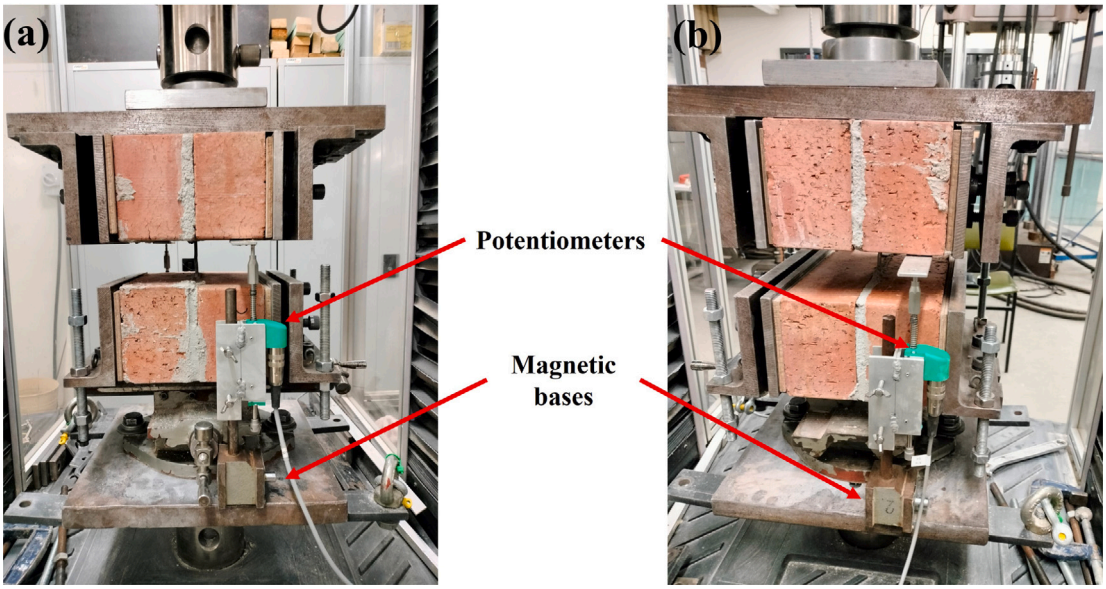

Fig. 3. (a) Front and (b) back views of the testing arrangement for compression loading.

was likely due to the construction quality of the sample, where the tie was not fully embedded in mortar, causing the corrugated end of the tie to debond within the mortar easily. During compression testing, no mortar crushing was observed, including the cases of interface buckling and piercing.

In Fig. 7, a multi-linear idealised curve is presented alongside the 10 load–displacement curves observed during compression testing. Five points were defined accordingly to capture the tie behaviour under compression: (point A) mean peak load was calculated as 2.95kN and the corresponding mean peak displacement (point A') was 0.91 mm, (point B) mean load at a fixed displacement of 4 mm, (point C) mean load at a fixed displacement of 10 mm, and (point D) mean load at a fixed displacement of 25 mm, corresponding to the stopping point of the compression test when the cavity displacement exceeded half of the cavity width. The fixed displacements for points B to D were selected based on visual inspection of the stiffness change in the load–displacement curves. The multi-linear ideal curves were derived to approximate the experimental load–displacement curves, since it provides a controllable mathematical representation of the stress–strain relationships, capturing the complex non-linear response in a multi-linear form. While other potential exponential functions may be applicable in this context, a multi-linear model facilitates the integration into the finite element analysis, enabling convenient stiffness calculation of the ties under compression and tension. The distinct points were selected to best reflect the overall trend of stiffness change in the load–displacement curves.

The interface buckling and piercing failure mechanisms are both plausible in real cavity walls due to variability in workmanship. The peak loads and the corresponding peak displacements for all 10 specimens were included in the subsequent analysis regardless of failure mechanisms to capture all different types of tie failure due to variability in tie construction. However, interface buckling and piercing failure mechanisms exhibited significantly different post-peak characteristics compared to the typical buckling failure. Hence, the determination of potential outliers for the post-peak characteristic points was performed according to the outlier assessment described in Appendix A of AS3700:2018. The outlier assessment indicated that only the load values at point C for the two samples were rejected. Without the exclusion of outliers, the post-peak average response within the multi-linear idealised curve would be distorted, especially the statistical characteristics of point C.

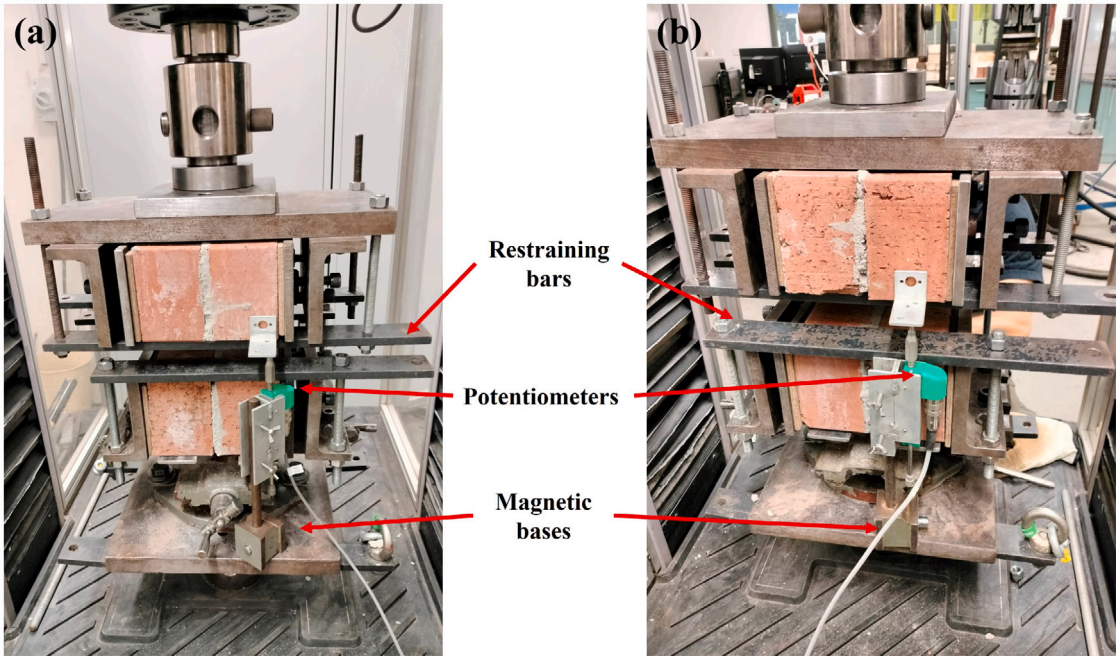

Fig. 4. (a) Front and (b) back views of the testing arrangement for tension loading.

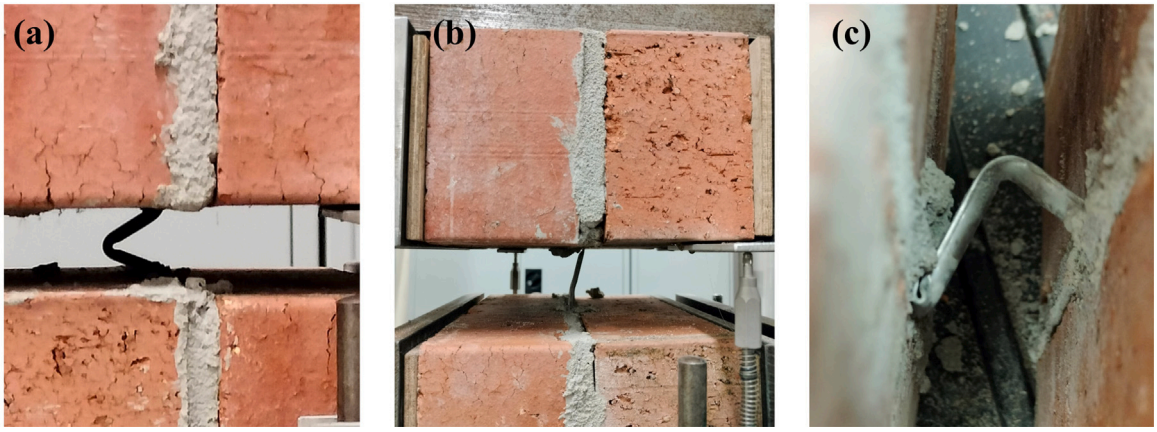

Fig. 5. (a) Typical axial buckling failure of tie under compression loading. (b) Slight offset was observed before the compression loading sequence for one of the samples and (c) a close up view of the corresponding interface buckling failure.

2.4. Tension test results

The remaining 10 brick-tie-brick subassemblies were tested under tension loading. The failure mechanism for tension loading was identical for all samples, resulting in tie pullout failure. No yielding or tie fracture was observed, suggesting that the ties were stronger compared to the bond between the mortar and the ties. The tie pullout failure mechanism is shown in Fig. 8.

Another idealised multi-linear curve to capture the tie behaviour under tension is shown in Fig. 9 along with the 10 tension load–displacement curves. Before introducing the characteristic points that define the idealised curve, attention is drawn towards the larger variability compared to the compression loading case. In Fig. 9, some of the load–displacement curves showed a sharp drop in load immediately after the peak load, likely due to the debonding between the tie and mortar joint. In addition, a clear trend of multiple peaks was observed after testing five samples. In order to investigate the complete tie behaviour, the remaining tension tests were extended to apply the tension loading until the ties were completely disconnected from the brick couplet. The load–displacement curves for the remaining five extended loading samples are shown in Fig. 10, where multiple peaks are clearly evident. The observed sinusoidal behaviour in the tensile regime was attributed to the phenomenon where the corrugated end of the embedded tie slid through the mortar and produced intermittent resistance due to the corrugated end design. The distance between the peaks corresponded to the flattened corrugation pitch length. Note that the displacement axes in Figs. 9 and 10 include the combined strain effect and slippage in the tie.

Using a similar strategy to idealise the tie behaviour under tension, five characteristic points were defined: (point A) mean load at a fixed displacement of 1.5 mm, (point B) mean peak load was calculated as 3.76kN and the corresponding mean peak displacement (point B') was 7.00 mm, (point C) mean load at a fixed displacement of 15 mm, and (point D) mean load at a fixed displacement of 25 mm. Point A was specifically selected at a displacement of 1.5 mm since the tie strength shall be taken as the force causing the tie failure or 1.5 mm deflection, whichever is lesser according to AS2699.1:2020. In addition to the peak load and displacement characteristic point (points B and B'), a similar rationale was incorporated to reject outliers, and one sample at points A and D was deemed as outlier. In order to avoid overfitting the

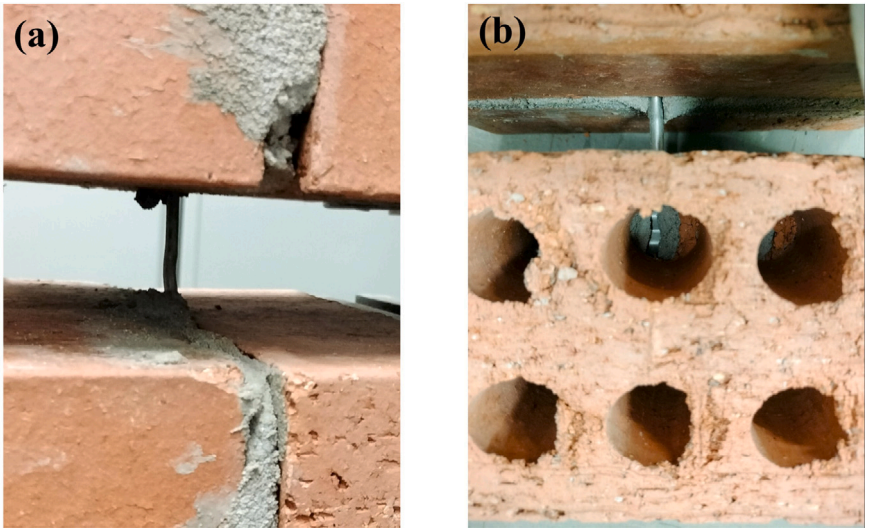

Fig. 6. (a) Piercing failure occurred and the tie remained straight after the test, (b) the tie could be seen from the top view, showing the lack of tie embedment in the mortar.

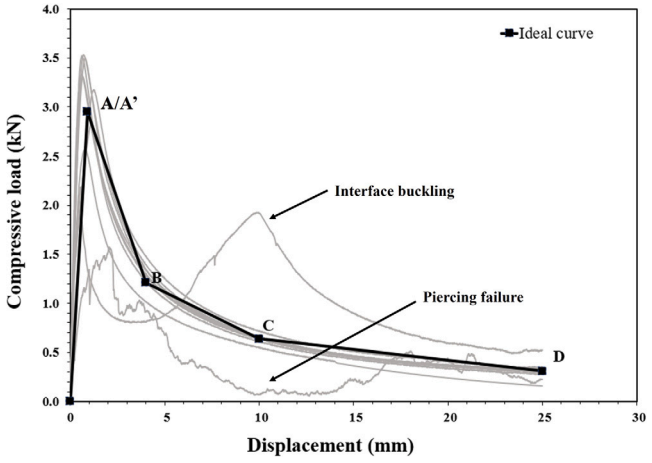

Fig. 7. Multi-linear idealised curve for compression test.

idealised curve with too many characteristic points, the residual multi-peak behaviour was not modelled, and an average residual strength was assumed as shown in Fig. 9.

In summary, a multi-linear idealised curve was obtained that describes the cavity wall tie behaviour under both compression and tension. Each characteristic point was defined by calculating the mean load values at the selected displacements and the corresponding mean displacement for the peak loads, excluding outliers. The next step is to further analyse the statistical parameters for each characteristic point to assign the best probability distribution, and develop an appropriate probabilistic model while quantifying the inherent variability of the cavity wall ties.

3. Probabilistic analysis

Maximum likelihood estimation was used to fit various probability distributions to the data sets of all characteristic points, including the tie strengths and the displacements at peak tie strengths. The Anderson–Darling (A-D) test [21] at the 5% significance level was used to evaluate unsuitable distributions. Then, a qualitative goodness-of-fit assessment was performed as outlined by Stewart and Lawrence [13], focusing on the lower tail of the inverse cumulative distribution function (CDF^{-1}), as that part of the distribution most strongly governs the failure of the system. The A-D test was specifically selected because this particular test places more emphasis on the tail distribution [22], ensuring a more robust and conservative prediction for weaker ties. The probability distributions under investigation include Gaussian (Normal) (N), Lognormal (LN), Extreme Value Type III (Weibull) (Wb) and Extreme Value Type I (Gumbel) (Gu) distributions.

3.1. Compression loading

The statistical parameters such as the mean and coefficient of variation (COV) for the characteristic points along with the best-fit probability distribution are summarised in Table 1. The fitted probability distributions and the corresponding CDF^{-1} plots for the five characteristic points (points A to D for variable tie strengths, and point A' for variable displacement) are presented in Figs. 11–15. A perfect fit of the distribution is demonstrated when the CDF^{-1} aligns with the 45-degree line. In assessing the goodness-of-fit, particular consideration of the lower tail of the examined probability distributions was made, as this region corresponds to weaker than average structural resistance, and therefore relates to a structural element with a greater probability of failure. The adopted distribution for each characteristic point was plotted in black, while the remaining ones were plotted in grey for clarity.

Based on the CDF^{-1} plots, Normal and Lognormal distributions were found to be the best-fit distribution for the characteristic points. Due to a limited sample size, there is insufficient statistical evidence to prefer one distribution over the other based on the CDF^{-1} plots alone. Hence, Lognormal distributions were adopted for all characteristic points for modelling convenience and also to avoid negative tie strengths and peak displacements, ensuring that the sampled tie strengths and peak displacements at a later stage still followed the same observed physical behaviour. Note that the Lognormal distributions adopted in the current study are subject to revision following more extensive physical testing to address the uncertainty in determining the most suitable probabilistic distribution.

3.2. Tension loading

Similar analyses were conducted on the characteristic points of the tie strength under tension loading. The summary of the statistical parameters and the result of the A-D test to fit various probability distributions are summarised in Table 2, while the fitted probability

Fig. 8. Tie pullout failure under tension loading.

Table 1
Summary of the statistical parameters and the selected probability distribution for tie characteristic points under compression loading.

Loading type	Characteristic point	Sample size	Mean	COV	Selected distribution
Compression	A (Peak)	10	2.95 kN	0.22	LN
	A'	10	0.91 mm	0.51	LN
	B	10	1.21 kN	0.18	LN
	C	8	0.64 kN	0.08	LN
	D	10	0.31 kN	0.30	LN

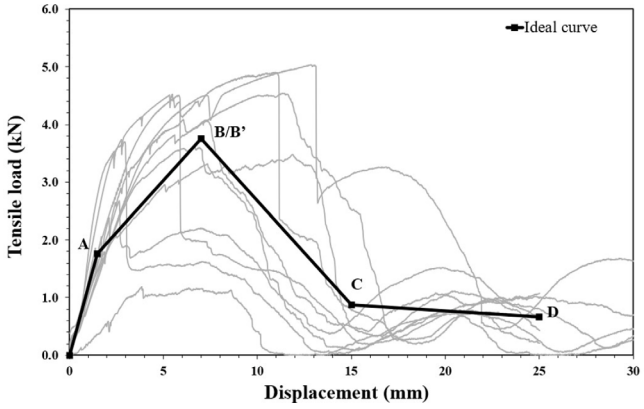

Fig. 9. Summary of tension test result up to 30 mm of cavity displacement.

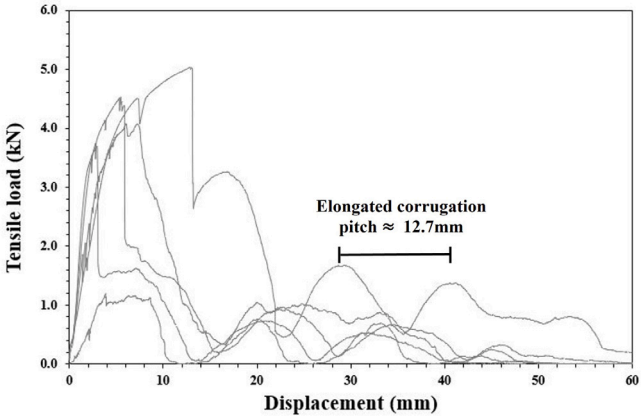

Fig. 10. Load–displacement curves of the samples that went through extended tension loading sequence up to 60 mm of displacement.

distributions and the corresponding CDF^{-1} are shown in Figs. 16–20. According to the same rationale used above to select the best-fit distribution, Lognormal distribution was deemed the best fit to model all tensile characteristic points based on their suitability and to maintain a convenient modelling approach.

The trend of higher variability of the statistical parameters for the tension case compared to the compression case was observed, especially Points B' and C with COV of 0.51 and 1.22 respectively. The high COV values could imply that the accuracy of multi-linear approximation to represent the mean tensile tie behaviour is limited. Using this model, fixed displacements were manually selected as characteristic points based on a visual inspection of the overall trend of stiffness change in the load–displacement curves, except for the displacement at peak load. Since the compressive load–displacement curves mostly followed a similar trend, the multi-linear approximation worked reasonably well for the compression case. However, the brittle nature of the tensile tie pullout failure was highly variable, causing the tensile characteristic points to be highly dependent on the selection of the appropriate displacement and their respective load values.

3.3. Correlation analysis

After determining the appropriate probability distributions to describe the data sets, a correlation analysis was conducted to investigate

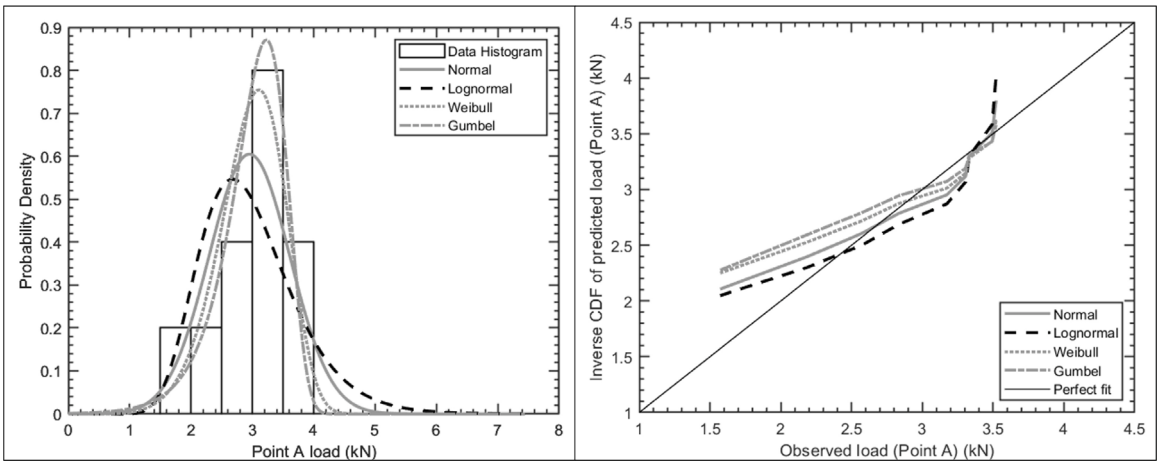

Fig. 11. Fitted probability distributions and CDF^{-1} of the tie peak compressive load (point A).

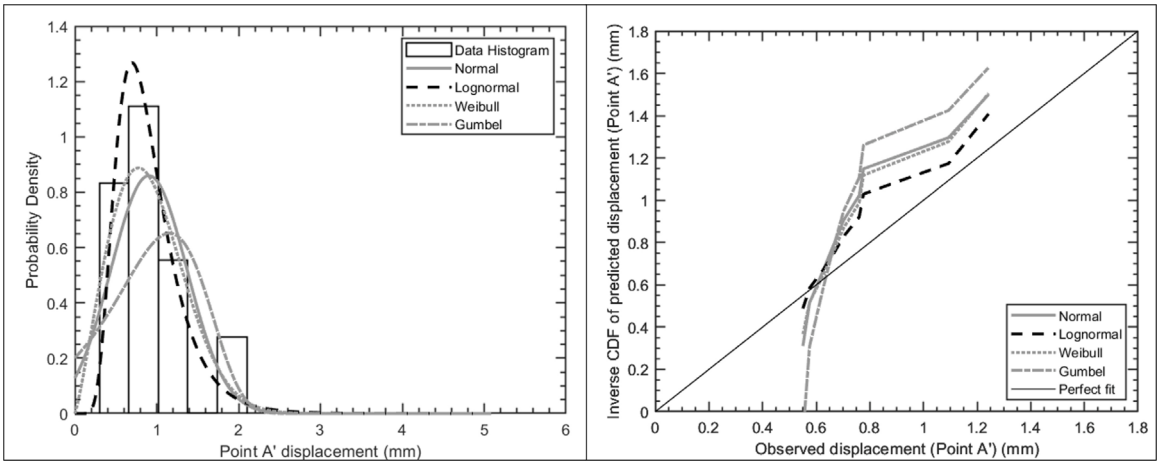

Fig. 12. Fitted probability distributions and CDF^{-1} of the tie displacement at peak compressive load (point A').

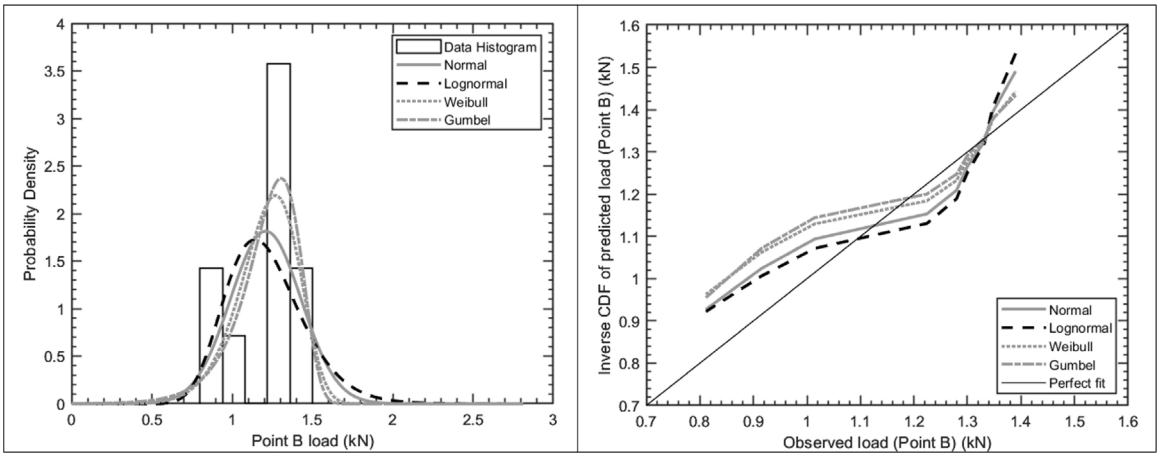

Fig. 13. Fitted probability distributions and CDF^{-1} of the tie compressive load at 4 mm (point B).

the relationship between the characteristic points. A total of four combinations were investigated for each loading type, where the relationships between tie strength characteristic points (points A and B, points B and C, points C and D) as well as the relationship between the peak load and the corresponding peak displacement (points A and A' for compression and points B and B' for tension) were considered. The correlation between characteristic points was examined using Pearson's correlation coefficient [23] as shown in Eq. (1).

$$\rho_{xy} = \frac{\sum_{i=1}^{n}(x_i - \bar{x})(y_i - \bar{y})}{\sqrt{\sum_{i=1}^{n}(x_i - \bar{x})^2 \sum_{i=1}^{n}(y_i - \bar{y})^2}} \tag{1}$$

where n is the number of data, x_i and y_i are the ith number of data, $\bar{x}$ and $\bar{y}$ are the sample means of the two data sets. $\rho = \pm 1$ indicates a full correlation while a value of zero indicates that there is no correlation

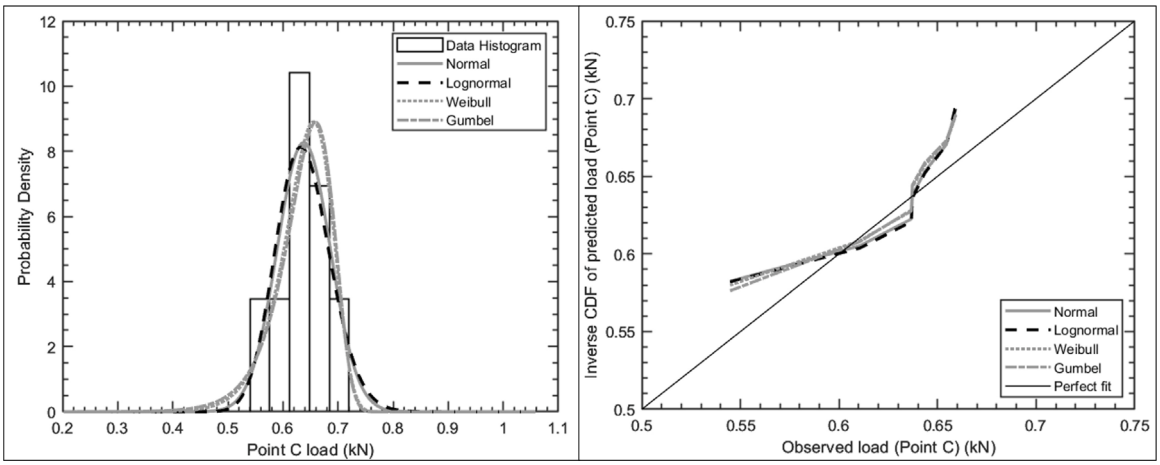

Fig. 14. Fitted probability distributions and CDF^{-1} of the tie compressive load at 10 mm (point C).

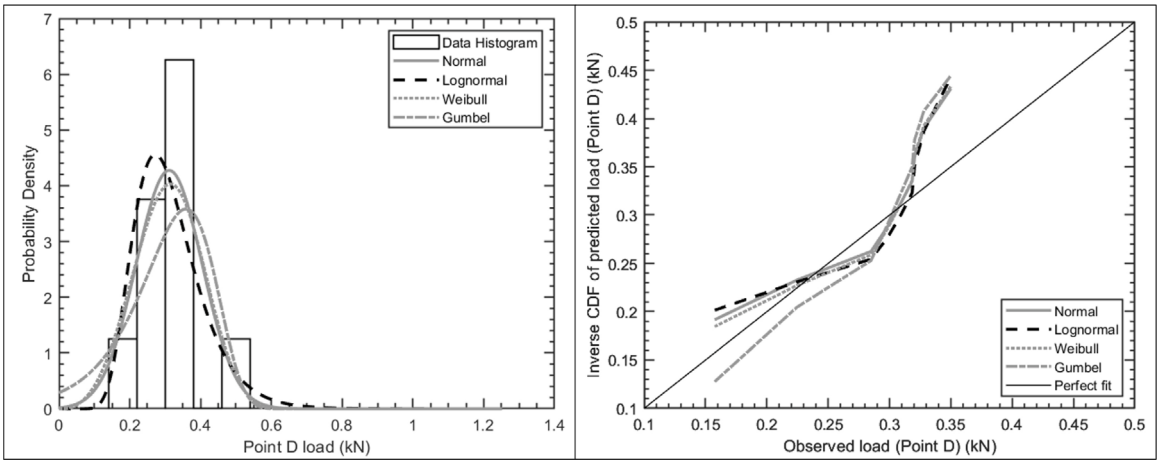

Fig. 15. Fitted probability distributions and CDF^{-1} of the tie compressive load at 25 mm (point D).

Table 2
Summary of the statistical parameters and the selected probability distribution for tie characteristic points under tension loading.

Loading type	Characteristic point	Sample size	Mean	COV	Selected distribution
Tension	A	9	1.76 kN	0.28	LN
	B (Peak)	10	3.76 kN	0.31	LN
	B'	10	7.00 mm	0.51	LN
	C	10	0.87 kN	1.22	LN
	D	9	0.66 kN	0.48	LN

between the two data sets. The calculated correlation coefficients and the corresponding scatter plots are summarised in Tables 3 and 4.

From Table 3, all four combinations of the characteristic points under compression loading showed a strong correlation with ρ greater than 0.85 for the tie strengths, while a moderate negative correlation of −0.64 was observed between the mean peak compressive load and its corresponding displacement. The correlation coefficient between points B and C was calculated as 0.98, indicating an extremely strong linear relationship. The correlation coefficient was further rounded to 1.00 for modelling simplicity, as the negligible difference is unlikely to influence the probabilistic analysis results. The p-values were also evaluated to determine the statistical significance of the computed correlation coefficients. From Table 3, all p-values were below 0.05, indicating that the null hypothesis of no correlation could be rejected at the 5% significance level, suggesting that the observed correlations were all statistically significant. The correlation relationship was further considered in the next stage when computing the conditional mean and standard deviation of the characteristic points under compression loading.

From Table 4, the computed correlation coefficients for the tension data set ranged from 0.03 to 0.71. ρ_{AB} was obtained as 0.03 with a p-value of 0.93, which is considered statistically insignificant and excluded from further analysis. However, the remaining correlation coefficients indicated moderate to high correlations. Although the p-values for the two of the remaining correlation coefficients slightly exceeded 0.05, they were still included for further analysis, since the p-values are indicative rather than definitive due to the reduced statistical power caused by the limited sample size.

By compiling the results of the probabilistic and correlation analyses, the probabilistic model of the cavity wall tie under investigation is summarised in Fig. 21, where the probability distribution, statistical parameters and the correlation coefficient between characteristic points are presented accordingly. Compared to the probabilistic model for the

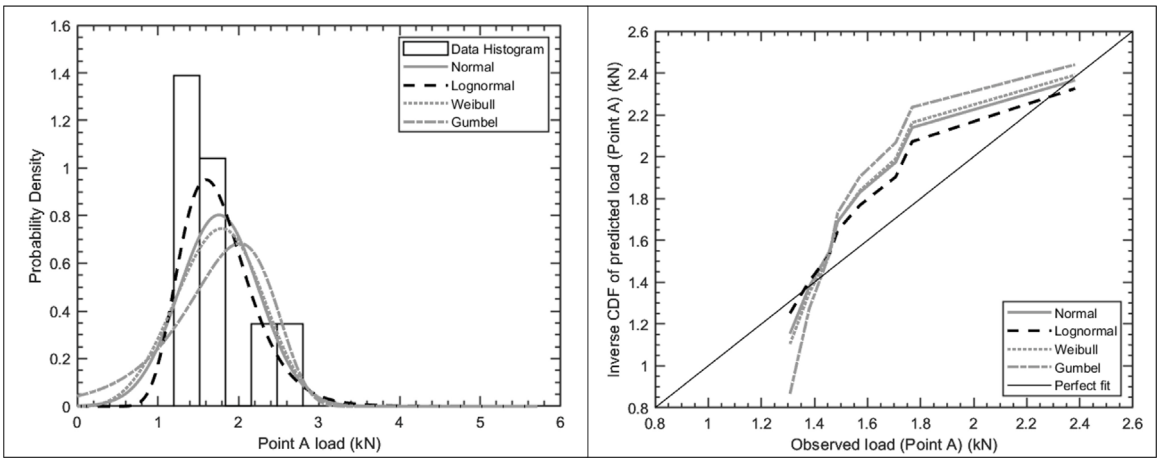

Fig. 16. Fitted probability distributions and CDF^{-1} of the tie tensile load at 1.5 mm (point A).

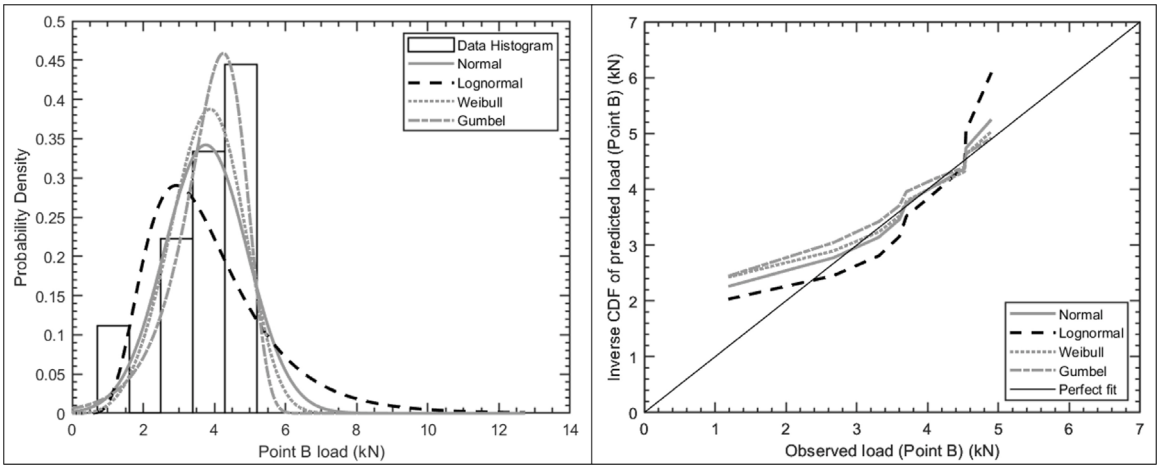

Fig. 17. Fitted probability distributions and CDF^{-1} of the tie peak tensile load (point B).

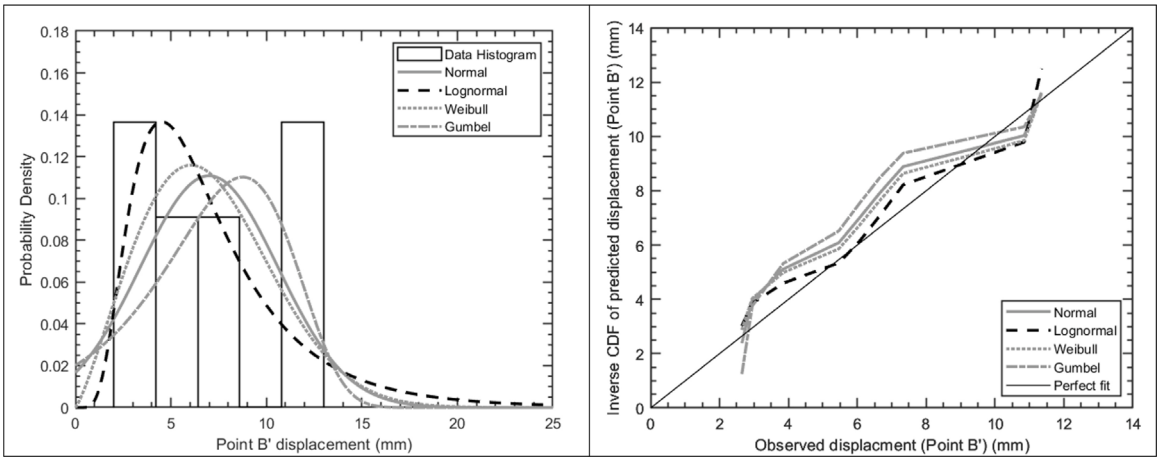

Fig. 18. Fitted probability distributions and CDF^{-1} of the tie displacement at peak tensile load (point B').

veneer wall tie defined by Muhit et al. [8], the mean peak stresses for the cavity wall tie under compression and tension loads were higher, consistent with its higher strength duty rating. The trend of the load–displacement curves for the cavity and veneer wall ties under compression was consistent. In contrast, the cavity wall ties exhibited a greater post-peak drop under tension at the specimen level, as evident in Figs. 9 and 10. The tensile responses of the cavity ties indicated a more brittle failure due to the tie pullout from the mortar, while the main failure mode for veneer wall tie was a more ductile nail pullout failure from the timber stud, as observed by Muhit et al. [8].

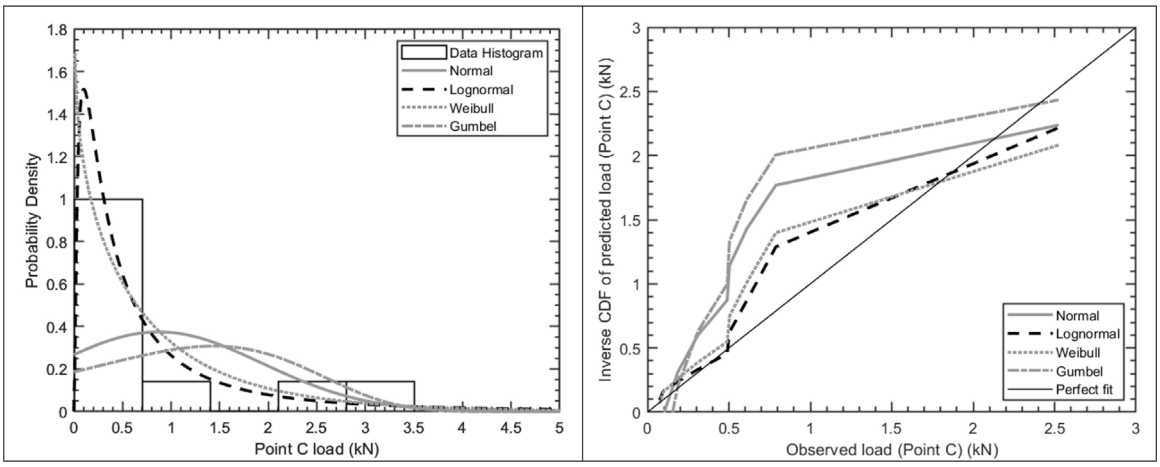

Fig. 19. Fitted probability distributions and CDF^{-1} of the tie tensile load at 15 mm (point C).

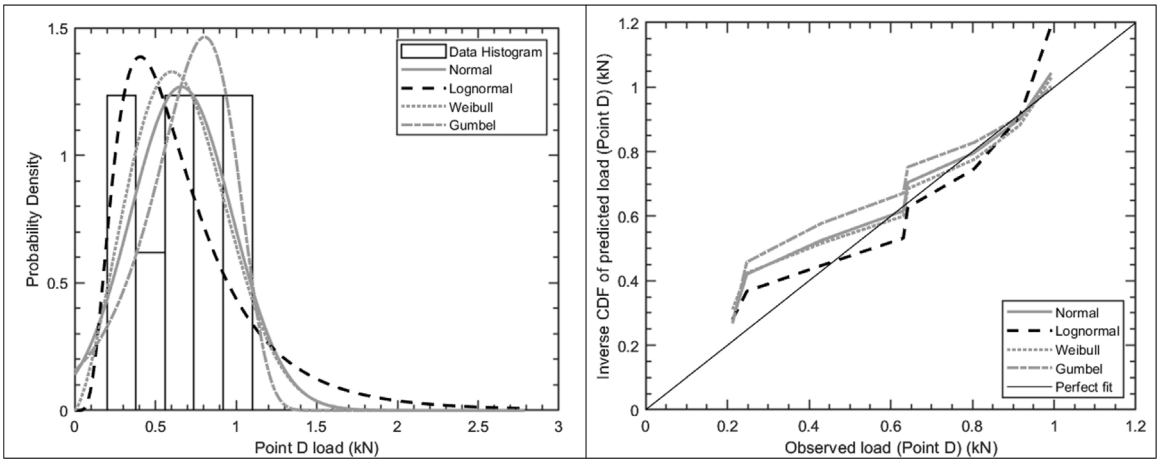

Fig. 20. Fitted probability distributions and CDF^{-1} of the tie tensile load at 25 mm (point D).

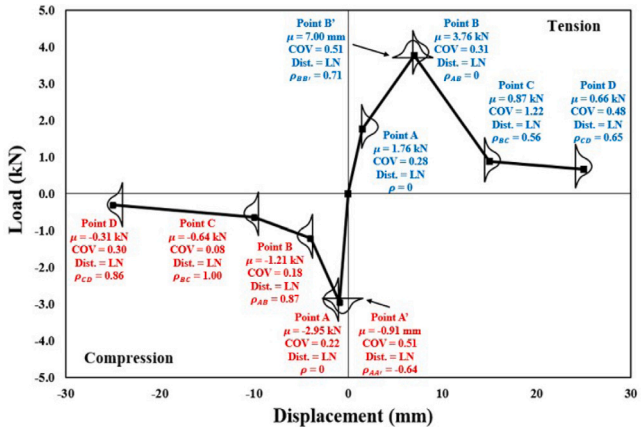

Fig. 21. Summary of probabilistic model for the cavity wall tie under compression and tension.

4. Numerical modelling of masonry cavity wall system

Based on the constructed probabilistic model of the cavity wall tie, deterministic and spatial stochastic finite element analyses were performed to investigate the influence of the variability of tie and masonry properties on the out-of-plane inward and outward loading capacities of a one-storey cavity wall.

4.1. Numerical modelling strategy

The one-storey cavity wall model was based on an actual cavity wall constructed in the laboratory, consisting of two wythes of brick walls. Each wall had nominal dimensions of 2400 mm long by 2322 mm tall by 110 mm thick, and a cavity width of 50 mm separating the two wythes. A total of 16 cavity wall ties were designed with vertical and horizontal spacings of 600 mm in accordance with AS3700:2018 to connect the two wythes of the brick wall, forming the cavity wall system. The cavity wall model under different loading conditions is shown in Fig. 22.

The one-storey cavity wall was modelled using the simplified micro-modelling strategy in DIANA FEA 10.8. While the mortar joints were not explicitly modelled, their mechanical behaviour along with the unit-joint interfaces was captured using the combined-cracking-shearing-crushing model, implemented through 2D planar interface elements (Q24IF) [24,25]. The geometric thickness of the mortar joints was incorporated into the brick units, forming expanded linear elastic continuum elements, which were modelled using HX24L elements. Each brick unit included a potential crack interface at mid-length with the same interface element types as the unit-joint interface using a linear softening model. A mesh density of 2 by 4 by 1 (length by thickness by height) was applied to each half brick unit as recommended in [14,17,26] to balance numerical accuracy and computational expense.

Table 3
Summary of the correlation assessment for compression data.

Relationship	Scatter plot	Correlation coefficient	p-value	Statistical significance
A and A'	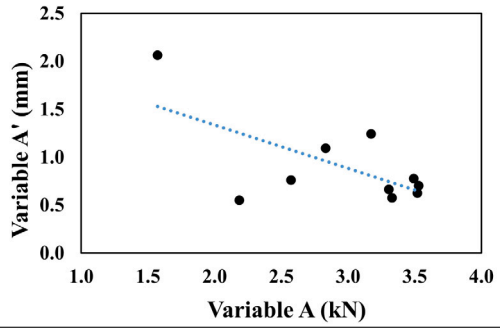	−0.64	0.0445	Yes
A and B	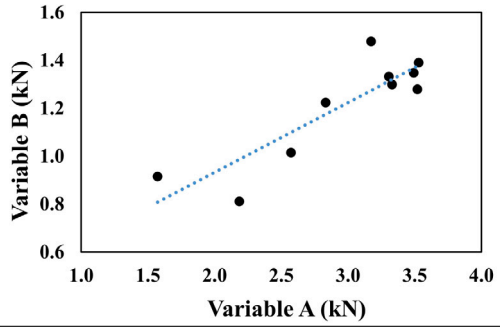	0.87	0.0010	Yes
B and C	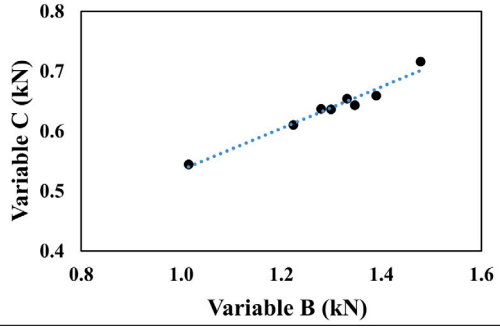	1.00	0.0001	Yes
C and D	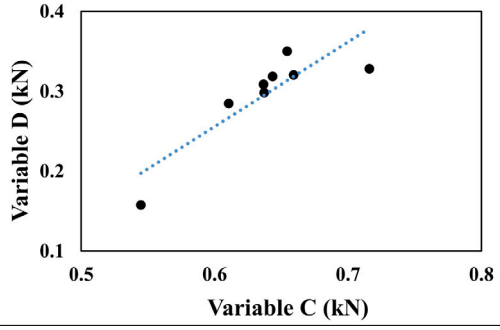	0.86	0.0059	Yes

Furthermore, the cavity wall ties were modelled as the enhanced 3D truss elements (L6TRU) using the uniaxial non-linear elastic material model. Given the clear strength softening behaviour of the ties, the uniaxial non-linear elasticity material model in DIANA software was selected purely as a convenient option to represent the ties using a user-defined stress–strain curve based on the cavity wall tie test results, rather than implying that the ties behave as fully elastic material. The modelling choice was deemed appropriate for the present study on monotonic loading (pushover analysis), where unloading–reloading and cyclic effects are not of interest. The stress–strain curve was defined as per Fig. 21, where the load values were converted to stresses by dividing the wall tie cross-sectional area of 9.5mm^2, and the strain values were obtained by dividing the displacements by the nominal cavity width of 50 mm. The current modelling strategies of the masonry cavity wall are consistent with the previous study conducted by Muhit et al. [17] for masonry veneer wall systems. Although the different failure mechanisms of the cavity wall ties were not explicitly represented in the FE model, the derived stress–strain relationship of the ties implicitly included the combined influence of the tie material behaviours, buckling and bond–slip interaction between the tie and the mortar.

Apart from the wall tie material properties, the out-of-plane bending capacity of the cavity wall is also governed by the tensile strength of the mortar joint. Hence, additional bond wrench (BW) and masonry compression (MC) tests were conducted in accordance with AS3700:2018 on specimens that were constructed concurrently with the cavity wall,

Table 4
Summary of the correlation assessment for tension data.

Relationship	Scatter plot	Correlation coefficient	p-value	Statistical significance
A and B	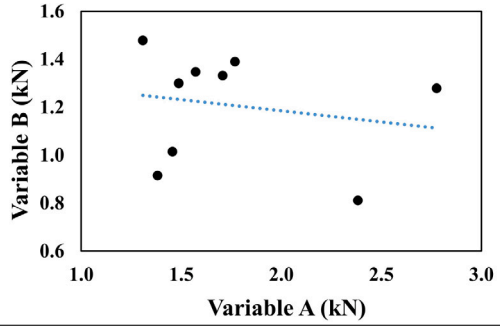	0.03	0.9311	No
B and B'	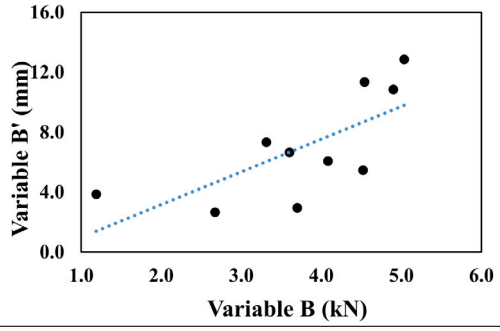	0.71	0.0220	Yes
B and C	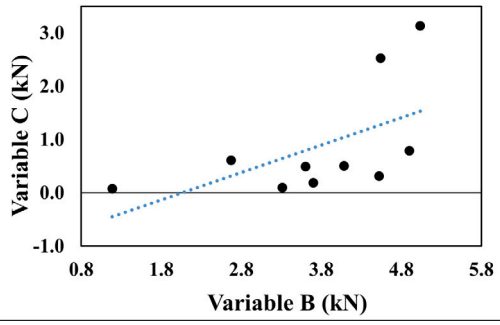	0.56	0.0891	Yes
C and D	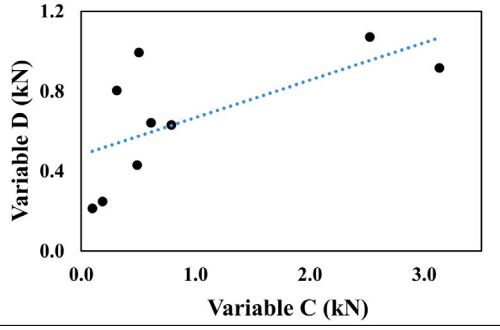	0.65	0.0588	Yes

and tested after approximately 4 weeks to obtain the mechanical properties of the masonry materials. In addition, other masonry properties were adopted based on previous testing done on similar masonry units and mortar mixes [27], and from the literature, as detailed in Table 5.

The bases of the cavity walls were restrained in all translational directions but were free to rotate. The top of the inner wythe was supported only in the out-of-plane translational direction, whereas the top of the outer wythe was unrestrained. Both ends of the wall tie were connected to the nodes on the inner and outer brick walls through the tying boundary conditions, ensuring that the displacement at one end of the wall tie matches the corresponding wall displacement. Non-linear structural analysis was conducted by applying uniform inward and outward pressure loads to the outer brick wall in the normal direction of its surface. Arc length control method with automatic step sizing approach was utilised to capture the load–displacement responses.

4.2. Spatial stochastic finite element modelling strategies

When conducting the deterministic finite element analysis, the masonry and tie properties were modelled using the deterministic values according to Table 5 and the mean characteristic points presented in Fig. 21 respectively, whereas spatial stochastic analyses utilised different material modelling strategies. Specifically, the probabilistic nature of the tie properties and the direct tensile strength of the unit-mortar interface were considered in the spatial stochastic finite element analyses, since both variables were the governing properties of the failure modes of the cavity wall under out-of-plane loading.

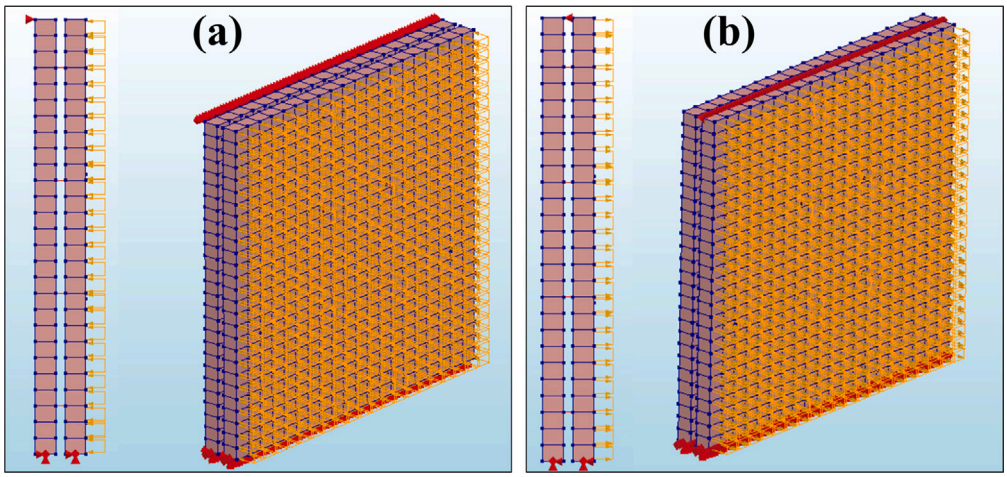

Fig. 22. Structural configurations of the cavity wall model subjected to (a) inward and (b) outward out-of-plane pressure loading conditions.

Table 5
FEA input of deterministic material properties for the cavity wall model.

Parameter	Value	Unit	Sources
Brick unit			
Elastic modulus	22734	N/mm^2	MC
Poisson's ratio	0.15	–	[28]
Density	1800	kg/m^3	[29]
Potential brick crack interface			
Linear normal stiffness	1000	N/mm^3	[28]
Linear shear stiffness	1000	N/mm^3	[28]
Direct tensile strength	1.332	N/mm^2	[27]
Fracture energy	0.037	Nmm/mm^2	[30]
Unit-mortar interface			
Linear normal stiffness	1269	N/mm^3	MC
Linear shear stiffness	529	N/mm^3	MC
Tensile strength	0.739	N/mm^2	BW,[31]
Tensile fracture energy	0.012	Nmm/mm^2	[28]
Cohesion (shearing)	1.137	N/mm^2	[27]
Friction angle (shearing)	0.86	Radians	[27]
Dilatancy angle (shearing)	0.55	Radians	[32]
Residual friction angle (shearing)	0.86	Radians	[32]
Confining normal stress (shearing)	−1.0	N/mm^2	[32]
Exponential degradation coefficient(shearing)	1.9	–	[32]
Masonry compressive strength (crushing)	13.6	N/mm^2	MC
Compressive fracture energy	20.18	Nmm/mm^2	[30]
Shear traction control factor (C_s)	9.0	–	[33]
Equivalent plastic relative displacement	0.007	mm	MC
Mode-II fracture energy factor, a	−0.8	mm	[32]
Mode-II fracture energy factor, b	0.05	N/mm	[32]

4.2.1. Probabilistic cavity wall tie strengths and displacements

The wall ties were considered to be statistically independent and sampled from the probabilistic model using the corresponding probability distribution for each characteristic point, while considering the correlation between the sampled characteristic points. During the sampling of the characteristic points, especially the peak loads and their corresponding displacements, restraints were imposed to ensure that all the sampled stress–strain curves followed a consistent physical material behaviour as observed in the experimental test. For example, the peak load in each stress–strain curve was set to always be the largest value, and the corresponding peak displacement was bounded between its neighbouring fixed displacements. The characteristic points were resampled if the conditions were not met. To justify that the imposed sampling constraints caused minimal statistical impact, the probability of the sampled peak tensile load being lower than the adjacent load values was calculated to be less than 3.5%. Meanwhile, the probabilities of the peak displacements in tension and compression falling outside their adjacent fixed displacements were only 3.31% and 0.04% respectively. An example of 16 sampled stress–strain curves is shown in Fig. 23 with the deterministic stress–strain curve as a reference.

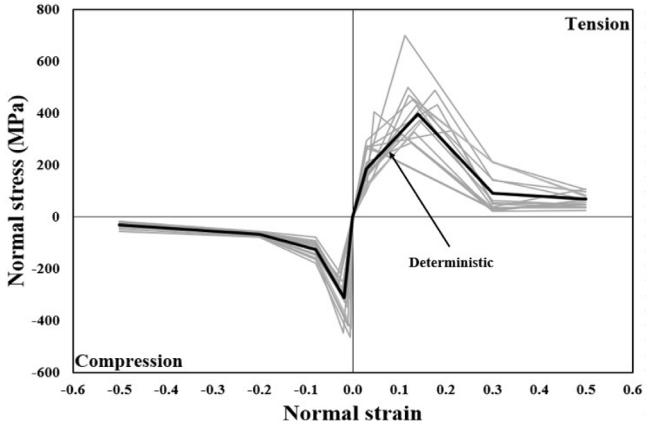

Fig. 23. The 16 stress–strain curves of the statistically independent cavity wall ties used in the first SFEA simulation are shown in grey, while the deterministic stress–strain curve is shown in black as a reference.

4.2.2. Probabilistic masonry properties

Since the tensile cracking of the mortar joint governs the behaviour of a cavity wall under out-of-plane loading, the direct tensile strength of the unit-mortar interface was also treated as a probabilistic variable on a joint-by-joint basis. Based on the bond wrench test results, the flexural tensile strength was converted to direct tensile strength by dividing a fixed ratio of 1.5, as adopted in [14,15,26], resulting in a mean and standard deviation of direct tensile strength of 0.74 N/mm^2 and 0.15 N/mm^2 respectively. Lognormal distribution was chosen to model and sample the direct tensile strength values for each joint, based on its established use in earlier studies [34,35] and its continued support in more recent observations [36,37].

The bed joints are usually laid over multiple bricks at once, whereas the perpend joints are laid one by one independently. To reflect this realistic bricklaying process, a spatial correlation coefficient of 0.4 was considered when sampling the direct tensile strength of the bed joints along the same course height, as demonstrated in [9,28]. Meanwhile, the direct tensile strength of the perpend joints was considered to be statistically independent. Several other masonry properties are correlated with direct tensile strength (f_t), including tensile fracture energy

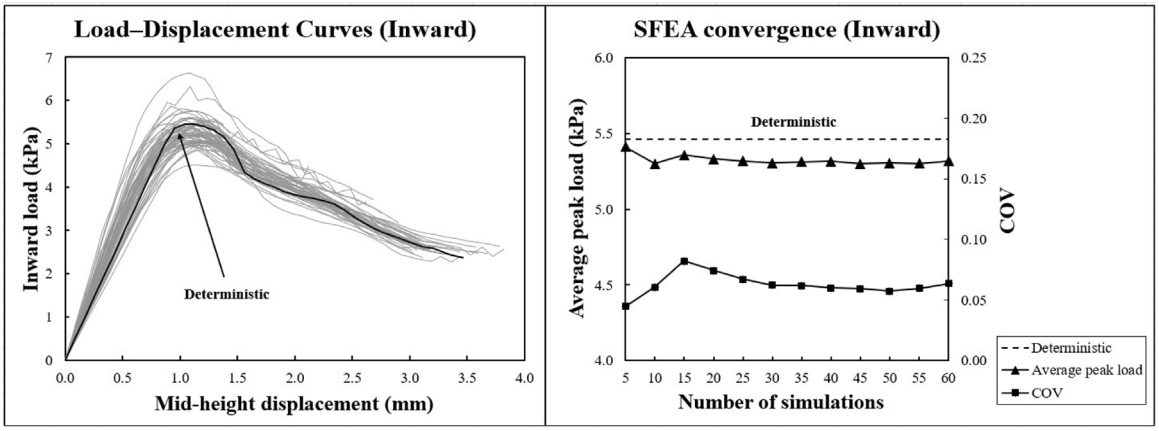

Fig. 24. Load–displacement curves of the cavity wall model under inward loading on the left, and the corresponding convergence statistic of the stochastic simulations on the right.

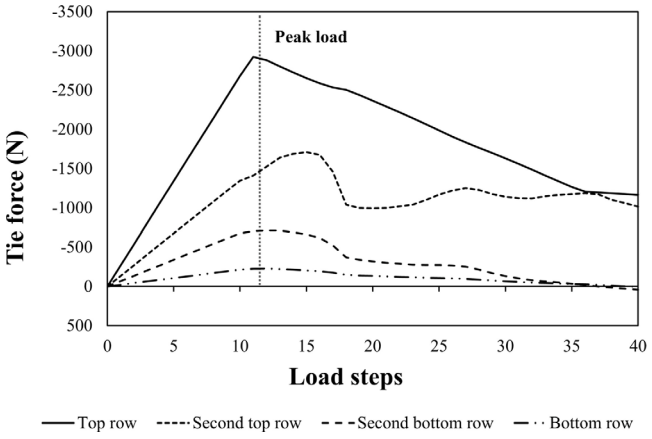

Fig. 25. The distribution of wall tie forces for the deterministic inward loading case.

(G_f^I), cohesion (c), masonry compressive strength (f'_m) and masonry compressive fracture energy (G_c).

Tensile fracture energy was treated as a dependent variable to the direct tensile strength in accordance with Eq. (2), which was derived by Heffler [28] based on the experimental testing of Van der Pluijm [31]. No shear triplet test was conducted for the current mortar batch, but cohesion is found to be correlated with the tensile strength of mortar joints, as evident in [38,39]. Therefore, a deterministic ratio of 1.54 was selected to estimate cohesion based on the direct tensile strength, as shown in Eq. (3). The ratio of 1.54 was calculated based on the ratio of cohesion to direct tensile strength obtained from the previous veneer wall test that utilised the same types of mortar and brick as the current cavity wall [27]. The fully correlated cohesion estimation approach was deemed adequate for the current study, as shear failure is not the main failure mode in the current study.

$$G_f^I = 0.01571 f_t + 0.0004882 \tag{2}$$

$$c = 1.54 f_t \tag{3}$$

While crushing is also not the primary failure mode, the values for masonry compressive strength and the corresponding compressive fracture energy were still calibrated according to Eqs. (4) and (5) [30]. For the masonry compression strength calculation, the ratio of the measured mean masonry compressive strength to the mean direct tensile strength was calculated and applied to the newly sampled direct tensile strength accordingly. The main reason for the calibration of the two properties based on f_t was to ensure that the tension cut-off criterion of the combined-cracking-shearing-crushing model was satisfied. As the cavity walls subject to out-of-plane bending are not subject to compression failures, the influence of this relationship shown in Eq. (4) on the global response of the modelled walls is minimal. For the remaining masonry properties listed in Table 5, deterministic values were used and no further spatial stochastic consideration was applied.

$$f'_m = \frac{f'_{m,mean}}{f'_{t,mean}} f_t = 18.38 f_t \tag{4}$$

$$G_c = 15 + 0.43 f'_m - 0.0036 {f'_m}^2 \tag{5}$$

4.3. Inward loading

The load–displacement curves under inward loading are presented in Fig. 24, where the black curve shows the result of the deterministic simulation while the remaining grey curves represent the results of the spatial stochastic simulations. A total of 60 spatial stochastic simulations were conducted, and the number of stochastic analyses was justified by the convergence of the mean and COV of the peak loads.

The deterministic simulation exhibited a clear peak load of 5.46 kPa along with an extended post-peak behaviour. The distribution of the tie forces is presented in Fig. 25, which shows that the top row of the wall ties reached the tie capacity near the peak load of the load–displacement response, indicating that the failure mechanism of the cavity wall under out-of-plane inward loading was governed by the failure of the top row of the ties. Meanwhile, masonry cracking was first observed in the inner brick wall along the height of the second top row of wall ties. As inward loading progressed beyond the peak load, the second top row of the wall ties took up only a marginal amount of load before converging towards lower load levels as the remaining ties. The behaviour indicated that the cavity wall system was unable to mobilise the resistance of the remaining ties due to progressive masonry cracking and softening. In the study conducted by Muhit [36] who modelled veneer wall systems under the same loading condition, two clear peaks were observed. The first peak was attributed to the cracking of outer brick veneer and the second peak was due to the buckling of the veneer ties. In contrast, only one peak was observed for the cavity wall system. The difference was due to the stiffness of the structural backings, where the timber frame that supports the outer brick veneer is more flexible compared to the inner brick wall for cavity wall systems. When the outer brick veneer cracks, the timber frame is able to deflect more and engage more ties to resist the inward pressure, while a stiffer inner brick wall would crack and collapse with excessive deflection without fully engaging all the ties.

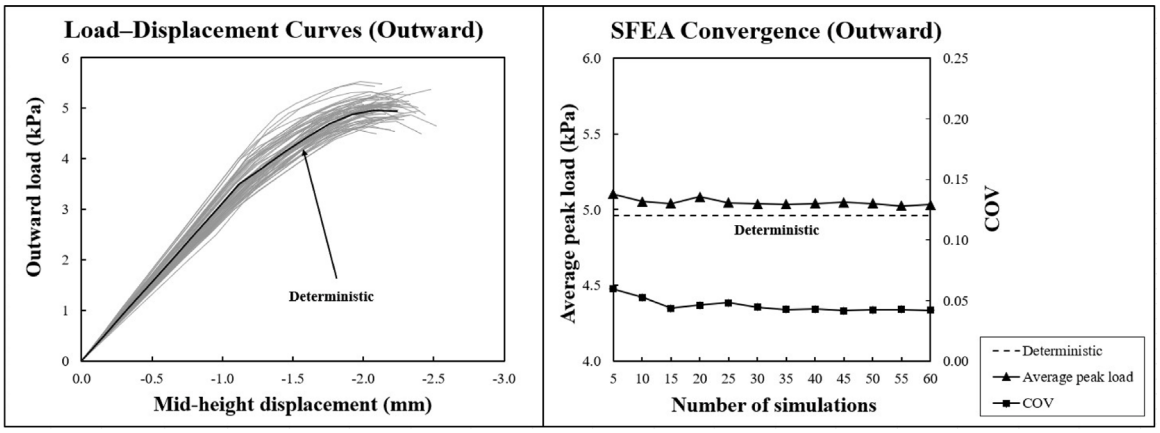

Fig. 26. Load–displacement curves of the cavity wall model under outward loading on the left, and the corresponding convergence statistic of the stochastic simulations on the right.

For the spatial stochastic simulations, the mean peak load for 60 simulations was 5.32 kPa, equivalent to a reduction of 2.6% compared to the deterministic result. This reduction is expected for a spatially variable SFEA as it introduced weak points in the model that a deterministic analysis ignores. The load–displacement curves for the stochastic simulations exhibited a similar post-peak behaviour, where the top row of the wall ties reached their respective capacities and governed the peak load of the cavity wall system under inward loading. The COV of the peak loads was monitored to evaluate the number of simulations needed to reach convergence. The results are plotted on the secondary vertical axis in Fig. 24, justifying the decision to include 60 simulations in the overall analysis, as the COV of the peak loads converged to 0.06 after 30 simulations.

4.4. Outward loading

The load–displacement curves for the outward loading case and the corresponding convergence of the stochastic simulations are presented in Fig. 26. The load–displacement curve for the deterministic model showed a peak load of 4.96 kPa but no extended post-peak behaviour. A closer examination of the tie forces revealed that all the ties did not reach their tensile capacity, indicating that the failure mechanism of the cavity wall system under outward loading was governed by the tensile strength of the unit-mortar interface. Masonry cracking initiated simultaneously near the four connection points between the inner brick wall and the ties at second top row. As the crack width increased further past the tolerable threshold, the analysis terminated, resulting in only one additional load step beyond the observed peak.

For the spatial stochastic simulations, the average peak load for 60 simulations was 5.03 kPa, equivalent to a slight increase of 1.4% compared to the deterministic result. The load–displacement curves for the stochastic simulations exhibited a similar trend, where around half of the stochastic simulations progressed one load step beyond the peak while the others terminated without a clear indication of a peak load. For those cases, the last load step was estimated as the peak load, suggesting that the mean peak load of the SFEA may be underestimated. In some stochastic simulations, the peak loads did not occur even when one of the ties at the top row reached its tensile capacity, indicating that the failure mechanism was still governed by the tensile strength of the unit-mortar interface. Similarly, the COV of the peak loads was monitored and the COV of the peak loads converged to 0.04 after 30 simulations, further confirming that 60 simulations were adequate for the current study.

Under outward loading, the difference between the mean peak load from the spatial stochastic simulations and the deterministic result was not substantial with only a 1.4% difference, but the slightly higher average may be attributed to a more efficient load sharing mechanism. When masonry cracking occurred at a weaker joint near the connection point with one of the wall ties at the second top row, more adjacent joints may have engaged and shared the load. In contrast, the mean peak load under inward loading was slightly lower than the deterministic result, possibly due to the limited ability to redistribute load once one of the top row ties failed, since there are only four variable ties at the top row.

The COV of the peak loads under the inward and outward loading conditions was 0.06 and 0.04 respectively. Although the difference was subtle, it supports the contrasting failure mechanisms observed between the two different out-of-plane loading directions. A slightly higher COV under inward loading reflects greater sensitivity to material variability, consistent with a tie-driven failure mechanism with only four top row ties to govern the inward loading capacity. In comparison, a slightly lower COV under outward loading aligns with the more distributed masonry-driven failure mechanism with the availability of multiple adjacent joints to share the load. Although speculative, the contrast highlights the complexity in cavity wall systems and the importance of utilising spatial stochastic analysis approach to investigate the interaction of spatially variable components that influence structural responses under different out-of-plane loading conditions.

5. Conclusions

In this study, the cavity wall ties were tested under axial compression and tension. Mean peak compressive load and its corresponding peak displacement were obtained as 2.95kN and 0.91 mm respectively, while 3.76kN and 7.00 mm were obtained for the tension case. Five characteristic points were defined for each loading case to capture the overall stiffness change of the cavity wall tie. Subsequent probabilistic analysis indicated that Lognormal distribution was suitable to describe each data set based on the A-D test at a 5% significance level. From the correlation analysis, statistically significant correlations were observed between the characteristic points of the compression and tension data sets, with the exception of the correlation between points A and B in the tension data set.

The probabilistic cavity wall tie model and the spatial variability of masonry properties were incorporated into the spatial stochastic finite element analyses, investigating the out-of-plane loading capacity of a single storey masonry cavity wall. Under inward loading, the failure mechanism was governed by the capacity of the ties at the top row, whereas masonry-governed failure was observed under outward loading. The stochastic results also showed slight differences in the mean and COV of the peak loads compared to their respective deterministic results, highlighting the influence of material variability. The use of

a spatial stochastic finite element analysis approach was instrumental in capturing subtle differences in the load-sharing mechanisms. Future work is planned to perform reliability-based assessment and quantify model error to strengthen the probabilistic evaluation of cavity wall systems that are subjected to out-of-plane loading.

CRediT authorship contribution statement

Chee Yin Lam: Writing – review & editing, Writing – original draft, Visualization, Validation, Software, Methodology, Investigation, Formal analysis, Data curation, Conceptualization. **Lewis J. Gooch:** Writing – review & editing, Validation, Software, Resources, Methodology, Formal analysis, Conceptualization. **Mark J. Masia:** Writing – review & editing, Validation, Supervision, Resources, Project administration, Methodology, Funding acquisition, Conceptualization. **Igor A. Chaves:** Writing – review & editing, Validation, Supervision, Resources, Project administration, Methodology, Funding acquisition, Conceptualization.

Declaration of competing interest

The authors declare the following financial interests/personal relationships which may be considered as potential competing interests: Igor Chaves and Mark Masia report financial support was provided by Australian Research Council. If there are other authors, they declare that they have no known competing financial interests or personal relationships that could have appeared to influence the work reported in this paper.

Acknowledgements

The financial support provided by The University of Newcastle and the Australian Research Council under the Linkage Project LP220100028 is gratefully acknowledged. The authors would like to thank Distinguished Professor Mark G. Stewart for his valuable input and guidance during the revision stage of this work. The authors are also grateful for the assistance provided by the laboratory staff at The University of Newcastle.

Data availability

Data will be made available on request.

References

[1] Choi YH, LaFave JM. Performance of corrugated metal ties for brick veneer wall systems. J Mater Civ Eng 2004;16(3):202–11.
[2] Reneckis D, LaFave JM, Clarke WM. Out-of-plane performance of brick veneer walls on wood frame construction. Eng Struct 2004;26(8):1027–42. http://dx.doi.org/10.1016/j.engstruct.2004.02.013.
[3] Page A, Simundic G, Masia M. Study of wall tie force distribution in veneer wall systems(stage 1). In: 11th Canadian masonry symposium. 2009.
[4] Zisi NV, Bennett RM. Shear behavior of corrugated tie connections in anchored brick veneer–wood frame wall systems. J Mater Civ Eng 2011;23(2):120–30.
[5] Rebelo F, Figueiredo A, Lopes GC, Ferreira TM, Vicente R. Development of retrofitting solutions: Remedial wall ties for masonry enclosure brick walls. Build (Basel) 2021;11(1):28. http://dx.doi.org/10.3390/buildings11010028.
[6] Arslan O, Messali F, Smyrou E, Bal IE, Rots JG. Experimental characterization of the axial behavior of traditional masonry wall metal tie connections in cavity walls. Constr Build Mater 2021;266:121141. http://dx.doi.org/10.1016/j.conbuildmat.2020.121141.
[7] Arslan O, Messali F, Smyrou E, Bal IE, Rots JG. Mechanical modelling of the axial behaviour of traditional masonry wall metal tie connections in cavity walls. Constr Build Mater 2021;310:125205. http://dx.doi.org/10.1016/j.conbuildmat.2021.125205.
[8] Muhit IB, Stewart MG, Masia MJ. Probabilistic constitutive law for masonry veneer wall ties. Aust J Struct Eng 2022;23(2):97–118.
[9] Heffler LM, Stewart MG, Masia MJ, Corrêa MRS. Statistical analysis and spatial correlation of flexural bond strength for masonry walls. Mason Int 2008;21(2):59–70.
[10] Stewart MG, Lawrence S. Structural reliability of masonry walls in flexure. Mason Int 2002;15(2):48–52.
[11] Lawrence S. Size effect in vertically spanning unreinforced masonry walls. In: 11th Canadian masonry symposium. 2009.
[12] Müller D, Förster V, Graubner C-A. Influence of material spatial variability on required safety factors for masonry walls in compression. Mauerwerk 2017;21(4):209–22.
[13] Stewart M, Lawrence S. Model error, structural reliability and partial safety factors for structural masonry in compression. Mason Int 2007;20(3):107–16.
[14] Li J, Masia MJ, Stewart MG, Lawrence SJ. Spatial variability and stochastic strength prediction of unreinforced masonry walls in vertical bending. Eng Struct 2014;59:787–97.
[15] Li J, Stewart MG, Masia MJ, Lawrence SJ. Spatial correlation of material properties and structural strength of masonry in horizontal bending. J Struct Eng 2016;142(11):04016112.
[16] Li J, Masia MJ, Stewart MG. Stochastic spatial modelling of material properties and structural strength of unreinforced masonry in two-way bending. Struct Infrastruct Eng 2017;13(6):683–95.
[17] Muhit IB, Masia MJ, Stewart MG, Isfeld AC. Spatial variability and stochastic finite element model of unreinforced masonry veneer wall system under out-of-plane loading. Eng Struct 2022;267:114674. http://dx.doi.org/10.1016/j.engstruct.2022.114674, URL https://www.sciencedirect.com/science/article/pii/S0141029622007684.
[18] Baibordy A, Yekrangnia M. Predicting pull-out strength and failure modes of metal anchors embedded in masonry structures using explainable machine learning models and empirical equations. Results Eng 2025;105287.
[19] Standards Australia. AS3700: Masonry structures. Sydney: Standards Australia; 2018.
[20] Standards Australia. AS2699.1: Built-in components for masonry construction, part 1: Wall ties. Sydney: Standards Australia; 2020.
[21] Anderson TW, Darling DA. A test of goodness of fit. J Amer Statist Assoc 1954;49(268):765–9.
[22] Ang AH-S, Tang WH. Probability concepts in engineering : Emphasis on applications in civil & environmental engineering. 2nd ed. Hoboken, N.J: John Wiley and Sons; 2007.
[23] Gibbons JD, Chakraborti S. Nonparametric statistical inference, In: Statistics, textbooks and monographs ; v. 168, 4th , rev. and expand New York: Marcel Dekker; 2003.
[24] Lourenço PB. Computational strategies for masonry structures [Ph.D. thesis], Delft University of Technology; 1996.
[25] DIANA FEA BV. DIANA Finite Element Analysis, Release Note 10.5. 2021.
[26] Isfeld AC, Stewart MG, Masia MJ. Stochastic finite element model assessing length effect for unreinforced masonry walls subjected to one-way vertical bending under out-of-plane loading. Eng Struct 2021;236:112115.
[27] Lam CY, Masia M, Chaves I, Hossain MA, Vazey J. Assessing wall tie deterioration in masonry veneer wall through vibration-based damage identification methods. Buildings 2025;15(8):1226.
[28] Heffler L. Variability of unit flexural bond strength and its effect on strength in clay brick unreinforced masonry walls subject to vertical bending [Ph.D. thesis], Australia: The University of Newcastle; 2009.
[29] Grimm CT. Clay brick masonry weight variation. J Archit Eng 1996;2(4):135–7.
[30] Lourenço PB. Structural masonry analysis: recent developments and prospects. In: Proceedings of 14th international brick and block masonry conference. 2008, p. 17–20.
[31] Van der Pluijm R. Non-linear behaviour of masonry under tension. Heron 1997;42(1):25–54.
[32] Petersen RB. In-plane shear behaviour of unreinforced masonry panels strengthened with fibre reinforced polymer strips [Ph.D. thesis], Australia: The University of Newcastle; 2009.
[33] Lourenço PB, Rots JG. Multisurface interface model for analysis of masonry structures. J Eng Mech 1997;123(7):660–8. http://dx.doi.org/10.1061/(ASCE)0733-9399(1997)123:7(660).
[34] Lawrence S, Cao H. Cracking of non-loadbearing masonry walls under lateral forces. Dublin, Ireland, vol. 2, 1988, p. 1184–94.
[35] Lawrence S, Lu JP. Cracking of brickwork walls with lateral loading. In: Asia-Pacific masonry conference. Singapore: DBCE; 1991.
[36] Muhit IB. Stochastic assessment of unreinforced masonry veneer wall systems subjected to lateral out-of-plane loading [Ph.D. thesis], Australia: The University of Newcastle; 2021.
[37] Gooch LJ. Stochastic assessment and structural reliability of spatially variable unreinforced masonry walls subjected to in-plane shear loading [Ph.D. thesis], Australia: The University of Newcastle; 2024.
[38] Masia MJ, Simundic G, Page AW. Assessment of the AS3700 relationship between shear bond strength and flexural tensile bond strength in unreinforced masonry. In: Proceedings of the 15th international brick and block masonry conference. 2012, p. 3–6.
[39] Gooch LJ, Masia MJ, Stewart MG, Lam CY. Statistical assessment of tensile and shear properties of unreinforced clay brick masonry. Constr Build Mater 2023;386:131578.